ACS APPLIED MATERIALS & INTERFACES

Research Article

www.acsami.org

Electrochemical and Structural Effects of In Situ Li_2O Extraction from Li_2MnO_3 for Li-Ion Batteries

Clement Jacob,[†] Jie Jian,[†] Qing Su,[‡] Stanislav Verkhoturov,[§] Renald Guillemette,[∥] and Haiyan Wang*[,†,‡]

[†]Department of Electrical and Computer Engineering, Texas A&M University, College Station, Texas 77843, United States

[‡]Department of Materials Science and Engineering, Texas A&M University, College Station, Texas 77843, United States

[§]Department of Chemistry, Texas A&M University, College Station, Texas 77943, United States

[∥]Department of Geology and Geophysics, Texas A&M University, College Station, Texas 77843, United States

ABSTRACT: Li_2MnO_3 is an attractive cathode material due to its low cost, nontoxicity and potentially high capacity. However, its electrochemical inactivity, its poor electronic conductivity, and uncertainty about its underlying mechanism have limited its development. In this work, an in situ technique for extraction of Li and O during deposition of the thin film cathode is developed to investigate structural and electrochemical effects in a controlled fashion. MnO_2 has been observed in samples with severe O and Li deficiency (capacity of 115 mAh g^{-1}), while Li_2MnO_3 cathodes with slight excess of O and Li (capacity of 225 mAh g^{-1}) can be synthesized by tuning growth conditions appropriately. Formation of a MnO_2 phase, especially in Li and O deficient structures, could be a possible reason for irreversible capacity loss in Li_2MnO_3 related materials. Further investigation into stoichiometric and microstructure variations enabled by this technique allows rapid investigation of Li_2MnO_3 as well as other Li-rich composites.

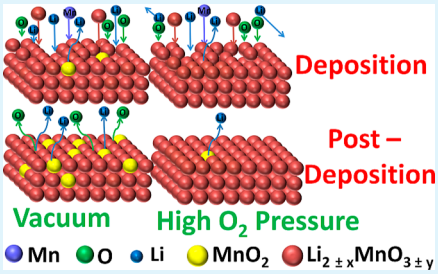

KEYWORDS: *Li_2MnO_3, battery, thin film, nonstoichiometry, MnO_2*

INTRODUCTION

Ever since they were first commercialized in 1991, Li ion batteries have been widely popular due to their high energy storage density. While recent advances have increased the capacity of anodes dramatically, the cathode continues to be constrained by capacity, cost, and environmental concerns.[1] The capacity for most cathode materials is limited to 140−170 mAh g^{-1}, while some of the elements, Co (in $LiCoO_2$), Ni (in $LiNiCoMnO_2$), etc., are expensive and toxic. As alternatives, manganese-based cathode materials, $LiMnO_2$,[2] $LiMn_2O_4$,[3] Li_2MnO_3,[4] etc., have been explored owing to their low cost and environmentally benign nature. However, $LiMnO_2$ and $LiMn_2O_4$ are significantly limited by their capacity and stability issues. Li_2MnO_3 has a high theoretical capacity of 459 mAh g^{-1} and has been used as a component in a Li-rich cathode with a demonstrated capacity of around 300 mAh g^{-1}.[5] Despite its great potential, Li_2MnO_3 requires preactivation by acid etching[5] or high voltage charging.[6] This activation is attributed to stoichiometric variation and associated phase changes. However, Li_2MnO_3-based cathodes are limited by poor cycle life, rate capability, and oxygen generation.[7] Rana and co-workers attributed the poor cycling life to repeated stress on the Li_2MnO_3 lattice structure due to proton exchange.[8] Thus, Li_2O removal by both acid etching and high voltage charging may be playing a role in structural degradation. Lee proposed that Mn occupies Li vacancies in a delithiated state.[9] So, it is plausible that excess Mn plays a role in cathode performance. It was also reported that Li ion dynamics can be tuned by changes in stoichiometry in Li_2TiO_3.[10] Fehr et al. reported that excess Li vacancies facilitate Li diffusion in Li_2TiO_3.[11] This approach may also prove advantageous for improving the performance of Li_2MnO_3 based cathodes. Clearly, a detailed stoichiometry variation study is needed.

In the past, such attempts have been mostly focused on either elaborate chemical synthesis methods to introduce small stoichiometry changes[12,13] or theoretical modeling to better understand underlying processes.[9] To our knowledge, there is no prior report on wide range stoichiometric variation for this material. We have previously shown that thin film cathodes can be useful in analyzing various aspects of battery performance.[14,15] In this work, we demonstrate a novel, fast, and flexible thin film, pulsed laser deposition (PLD) based approach to directly synthesize $Li_{2\pm x}Mn_yO_{3\pm y}$ with a wide range of stoichiometry by controlling Li and O content of the cathode during deposition. Such wide stoichiometry control is achieved by controlling the deposition parameter during the thin film deposition process. This method can be employed to improve the stability of the layered structure and ionic conductivity. Furthermore, the possibility of simultaneous removal of lithium and oxygen has been explored to electrochemically probe activation and irreversible capacity loss in Li_2MnO_3. Two extreme cases can be created, one with severe Li and O deficiency, thus effectively getting a Mn excess phase, and the other with excess Li. The structural and compositional

Received: October 16, 2014
Accepted: January 8, 2015
Published: January 8, 2015

DOI: 10.1021/am5071305
ACS Appl. Mater. Interfaces 2015, 7, 2433−2438

observations are correlated with corresponding electrochemical properties.

EXPERIMENTAL SECTION

Li_2MnO_3 target was prepared by mixing Li_2MnO_3 (Pfaltz & Bauer) with Li_2CO_3 (Alfa Aesar) in desired molar ratio. The powder was mixed using a high energy ball mill for 1 h and decomposed in a flowing Ar atmosphere at 350 °C. The resultant powder was then pressed into a pellet and annealed at 600 °C. The film was deposited using a PLD system with a 248 nm KrF laser source with a laser fluence of 1 J cm^{-2} at 10 Hz. The target substrate distance was set at 4 cm for all deposition. A polished stainless steel substrate with a gold coating was used for electrochemical testing, and c-cut sapphire substrates were used for TEM and XRD. While the conducting substrate is necessary for electrochemical evaluation, the single crystal sapphire substrate simplifies the TEM sample preparation process and crystal structure analysis of the film. The films were deposited at 750 °C under different oxygen partial pressure ranging from 0 to 100 mTorr. The samples were cooled at approximately 10 °C min^{-1} under different partial oxygen pressures. The details of the deposition conditions are listed in Table 1. The cathodes have an approximate

Table 1. Deposition Conditions for Different Cathodes

oxygen partial pressure (mTorr)	post-deposition pressure (Torr)
0	0
5	10
50	50
100	500

film thickness of 180 nm with a loading of ~70 μg cm^{-2}. XRD measurements were done on a PANalytical Empyrean 2 XRD system using a Cu Kα source with a 1/2° fixed diffraction slit and a 1 mm receiver slit.

SEM images were obtained on a FEI Quanta 600 field emission scanning electron microscope, and TEM and STEM images were taken on a FEI Tecnai G2 F20 ST field emission system and an aberration-corrected FEI Titan microscope equipped with a high brightness Schottky-field emission electron source operated at 300 kV, respectively. Wavelength dispersive spectroscopy to quantify composition of the films was carried out on a Cameca SX50 electron microprobe. An accelerating voltage of 15 kV and beam current of 20 nA was used for the measurements. Since Li cannot be measured directly, a difference method was employed to estimate Li content. The composition was further verified with secondary ion mass spectrometry (SIMS) using a Cameca IMS 4f ion microprobe. CR2032 coin cells were assembled in an Ar atmosphere (Glove Box, O_2 0.1 ppm, H_2O 0.1 ppm) with Li metal anode and Celgard 2400 separator. Ethylene carbonate/dimethyl carbonate (EC/DMC 1:2 by volume) with 1 M $LiPF_6$ salt was used as electrolyte. Cyclic voltammetry (50 μV s^{-1}) and battery cycling was carried out on an Arbin BT2000 system.

RESULTS AND DISCUSSION

The X-ray diffraction (XRD) patterns in Figure 1 present films grown on sapphire substrates under different conditions as summarized in Table 1. XRD data show that the films have a monoclinic structure and the peaks were indexed according to a $C2/m$ space group structure, Li_2MnO_3 (ICDD no. 202639). The bulk XRD is similar to the ICDD card. The films deposited on the c-cut sapphire substrates are highly textured with predominantly three preferred orientations. All samples show a strong (001) peak indicating that one of the preferred orientations is along the c-axis for the monoclinic phase. In addition, all the samples grown under partial oxygen pressure show a stronger $(20\bar{2})$ peak. The similarity between the diffraction patterns of the films deposited under 5, 50, and 100

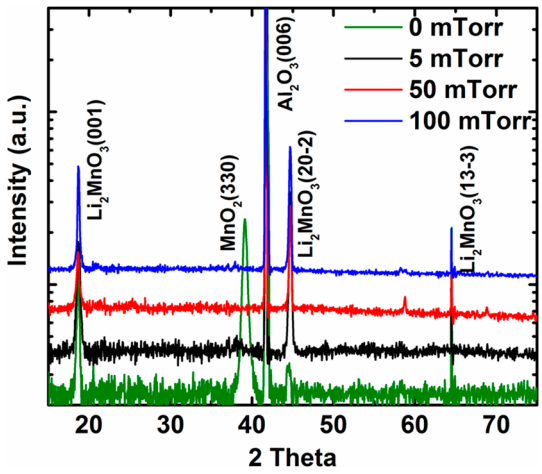

Figure 1. X-ray diffraction patterns of films deposited under different oxygen partial pressure.

mTorr suggests a stronger dependence on the post-deposition conditions rather than the partial pressure during deposition. Based on the diffraction pattern, the 50 mTorr sample has lattice parameters a = 4.89 Å, b = 8.44 Å, and c = 5.05 Å for β = 90.4°. This matches well with other reports in literature.[16] The vacuum-deposited sample shows an additional peak around 39°, which is likely to be either α-MnO_2 (330) (JCPDS 44-0141) or γ-MnO_2 (222) (JCPDS 44-0992). In the absence of further data, it is difficult to determine the exact structure of the phase. The broad peak indicates the poor crystallinity of the MnO_2, which might be due to coexistence of the two MnO_2 phases. This will be discussed further in the context of other measurements.

A detailed wavelength dispersive spectroscopy (WDS) study was conducted to determine compositional variation and the data for films on stainless steel substrates are summarized in the plot in Figure 2a. The stoichiometric sample was a pellet prepared using as-received powder to provide a baseline to compare the stoichiometric case; the oxygen to manganese (O/Mn) ratio in the vacuum sample is determined to be around 1.75. On the other hand, the 100 mTorr sample has an O/Mn ratio of about 3.25. Clearly, a large variation in oxygen content has been achieved under different deposition conditions. This is different from other works that passively observed Li_2O removal[17] and demonstrates active controlled removal of Li and O. The large deviation from the original stoichiometry observed for the 0 mTorr (vacuum) sample indicates the possible presence of a secondary MnO_2 phase, as suggested by the above XRD results. However, the amount of Li cannot be measured directly with WDS and therefore was calculated by comparing the difference. The Li to Mn (Li/Mn) ratio plot shows that the vacuum and the 100 mTorr samples are both Li deficient. To enable direct measurement of Li concentration, secondary ion mass spectrometry (SIMS) was further conducted to confirm the Li content in the films. and the results are shown in Figure 2b. The SIMS data is mostly consistent with the WDS result, and the 6Li profile clearly shows that the 0 mTorr sample contains the least Li followed by the 100 mTorr sample. Similar to the WDS result, the Li contents of the 5 and 50 mTorr samples are comparable. Under high vacuum, two mechanisms could result in Li deficiency. A lack of oxygen may cause the formation of metallic lithium or Li_2O during film deposition. This combined with a substrate

DOI: 10.1021/am5071305
ACS Appl. Mater. Interfaces 2015, 7, 2433−2438

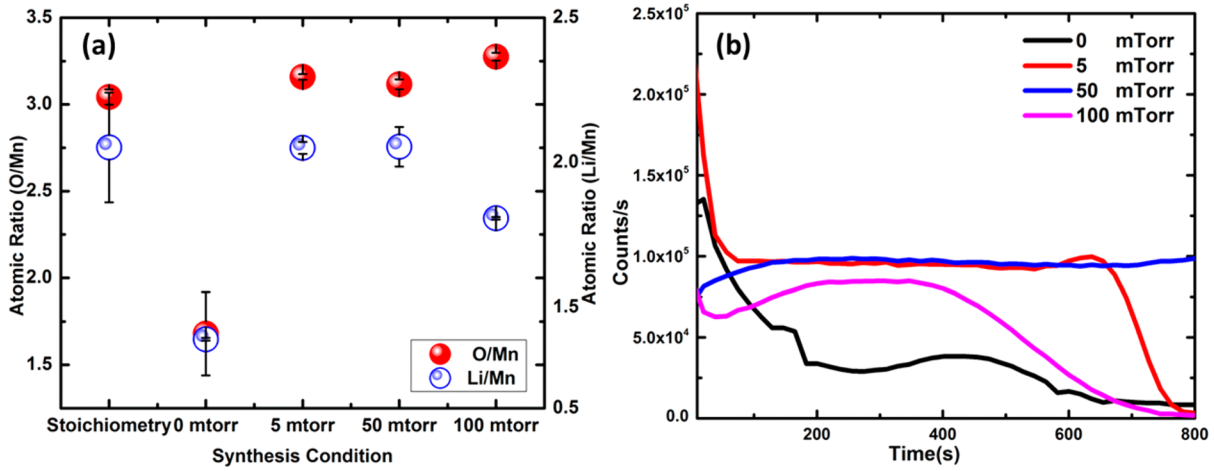

Figure 2. (a) Wavelength dispersive spectroscopy results indicating O/Mn and Li/Mn ratio of the stoichiometric pellet and films deposited under different oxygen partial pressure. (b) Secondary ion mass spectroscopy results for Li content for the different cathode films.

temperature of 750 °C and high vacuum could cause desorption of Li/Li_2O from the film. Under high oxygen partial pressure, the light Li ions get deflected by ambient oxygen molecules resulting in an oxygen deficient film. The Li_2O removal and MnO_2 formation that occurs during the film deposition can be depicted by the following reaction.

$$Li_2MnO_3 \rightarrow Li_2O\uparrow + MnO_2$$

Li_2O represents the various Li and O loss mechanisms described above, and the loss is indicated by arrow. The fraction of the Li_2MnO_3 that converts to MnO_2 and the loss of Li_2O are controlled by the deposition conditions. The mechanism resulting in stoichiometry variations is illustrated in schematic drawings in Figure 3. The 5 and 50 mTorr samples

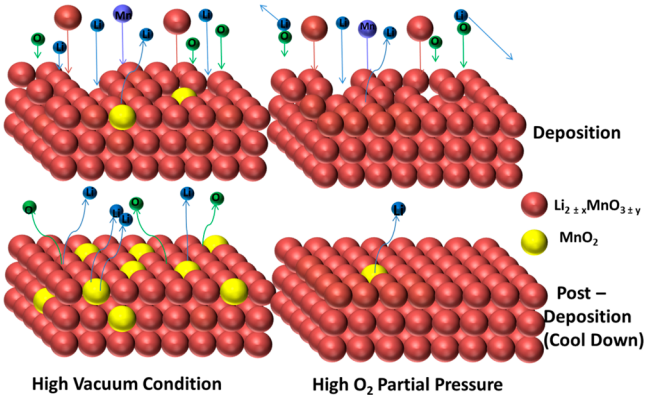

Figure 3. Model depicting deposition process and resulting stoichiometry for high vacuum and high oxygen partial pressure conditions.

are closer to the stoichiometric case. The composition data in combination with XRD results show that small stoichiometric variations lead to either Li or O deficient or rich films. Furthermore, a large reduction in any of the elements leads to the formation of secondary phases, such as MnO_2 observed in the vacuum case. The presence of MnO_2 further confirms that the removal of Li_2O was achieved as initially proposed. Further work on fine-tuning of the process to achieve intermediate stoichiometry between the vacuum and 5 mTorr samples is currently underway.

The effect of deposition parameters on surface morphology was investigated using scanning electron microscopy (SEM) and is shown in Figure 4 for (a) vacuum, (b) 5 mTorr, (c) 50

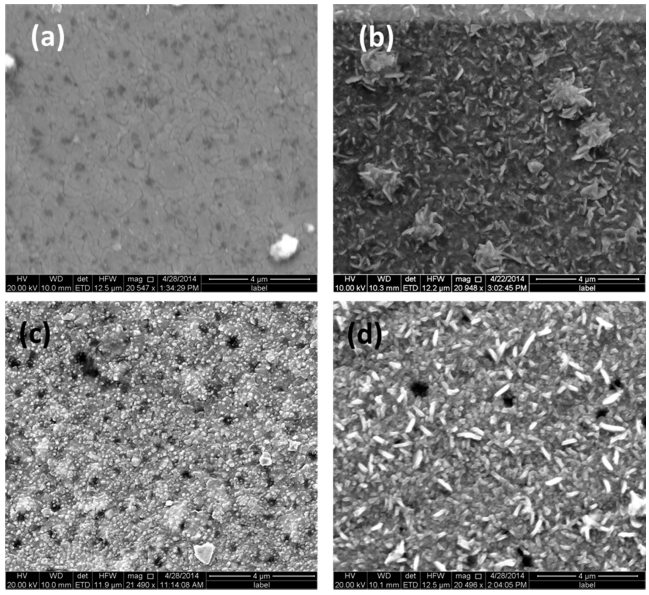

Figure 4. SEM images for films deposited under (a) vacuum, (b) 5 mTorr, (c) 50 mTorr, and (d) 100 mTorr.

mTorr, and (d) 100 mTorr. The surface of the vacuum sample (a) is quite smooth. Under higher partial pressures, the surface shows nanoplate like or sphere like features. For example, the 50 mTorr sample (c) shows nanospherical grains, which naturally maximize surface area. While the grain morphology will affect properties, for thin films the phase and stoichiometry of the film should dominate electrochemical performance. Transmission electron microscopy (TEM) micrographs of these samples were taken to investigate the microstructure properties further. The sapphire substrate provides a good reference to analyze the film and improves crystallinity of the film. Since the films were deposited at the same time on both Au-SS and sapphire substrates, the film composition and phase is similar on both substrates. The results for the 50 mTorr sample are shown in Figure 5. The TEM images show that the film is dense with large grains. The obvious lattice fringes

DOI: 10.1021/am5071305
ACS Appl. Mater. Interfaces 2015, 7, 2433−2438

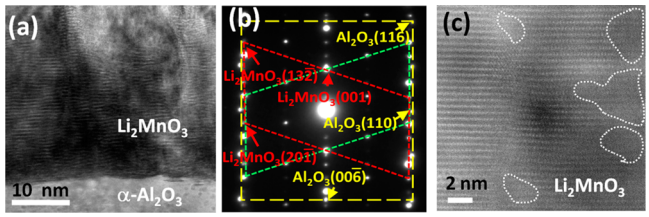

Figure 5. (a) TEM image, (b) SAED pattern, and (c) STEM image of sample deposited on c-cut sapphire at 50 mTorr partial pressure.

indicate obvious *c*-axis oriented film in this area on a c-cut sapphire substrate. Figure 5b shows the selected area electron diffraction (SAED) to confirm the phase and crystallinity of the samples. Based on the diffraction pattern, three sets of diffractions can be identified. The two sets of symmetric diffraction patterns, marked in red and green, are indexed as Li_2MnO_3, and the sapphire diffraction pattern is marked in yellow. No obvious impurity phases were identified in the diffraction pattern in this area. Obviously, Li_2MnO_3 (001) planes are parallel to the sapphire (006) planes, and the film shows good crystallinity, evident from the distinguished diffraction dots. Scanning transmission electron microscopy (STEM) images were also taken to resolve chemical disorder in the film. STEM under high angle annular dark field mode (HAADF) is also called *Z*-contrast where the image contrast is proportional to the atomic number *Z*. The image of the corresponding film (2f) shows some disordered structure with amorphous-like regions, possibly due to the presence of oxygen vacancies. STEM images indicate that the film composition is not uniform and localized defects are present even in the 50 mTorr samples.

The cyclic voltammetry results for the different cathodes are plotted in Figure 6a–d after an initial cycle to evaluate the effect of deposition conditions on electrochemical performance. All batteries show a redox peak pair around 4.2 V with the oxidation peak at 4.25 V and the corresponding reduction peak at 4.1 V. This is significantly lower than the standard peak associated with irreversible oxygen loss.[18] Moreover, the small gap in the oxidation and reduction potentials indicates that the associated redox pair is highly reversible. This is likely associated with Mn ions with different activation energies due to valence or atomic position in the crystal compared with the redox pair observed around 3 V. In fact this is very similar to the redox pair at 4.1 V attributed to a two-step extraction of Li reported by Rossouw and Thackeray in $LiMn_2O_4$.[19] The cathodes synthesized at higher partial pressures show a secondary oxidation–reduction pair at 3 and 2.75 V. This peak is generally attributed to Mn ion after a layer-to-spinel phase transformation.[20] The additional pair is likely to contribute to a higher capacity for films deposited under higher partial pressures. Increased partial pressure clearly results in stronger redox peak around 3 V. It is surprising because this peak is generally indicative of the activation of this cathode material, which in turn is normally associated with Li_2O removal. This aspect is further discussed in context of structural data below. Nevertheless, very limited cyclic voltammetry results are available in literature for Li_2MnO_3. These data confirm the importance of the 3 V redox reactions for good performance of the batteries to be seen in the following section.

Figure 7a shows cycling capability of the different cathodes at 0.1 C. The 50 and 100 mTorr samples show good cycling stability. The capacity and cycle life obtained for the 50 mTorr sample are better than those reported by several groups for Li_2MnO_3 cathodes.[7,12,21] The improved capacity is likely attributed to nonstoichiometry induced defects as reported previously.[7] Figure 7b shows the charge–discharge capacity of the different cathodes vs Li anode when cycled between 2.5 and 4.5 V at different *c*-rates. The cathode films deposited at 50 mTorr show the highest capacity, with a discharge capacity of 225 h/g at 0.05 C, which corresponds to extraction of 0.98 Li per formula. This is close to, but slightly higher than, the capacity of the 100 mTorr films. The high density of local defects observed in the STEM images may also be responsible

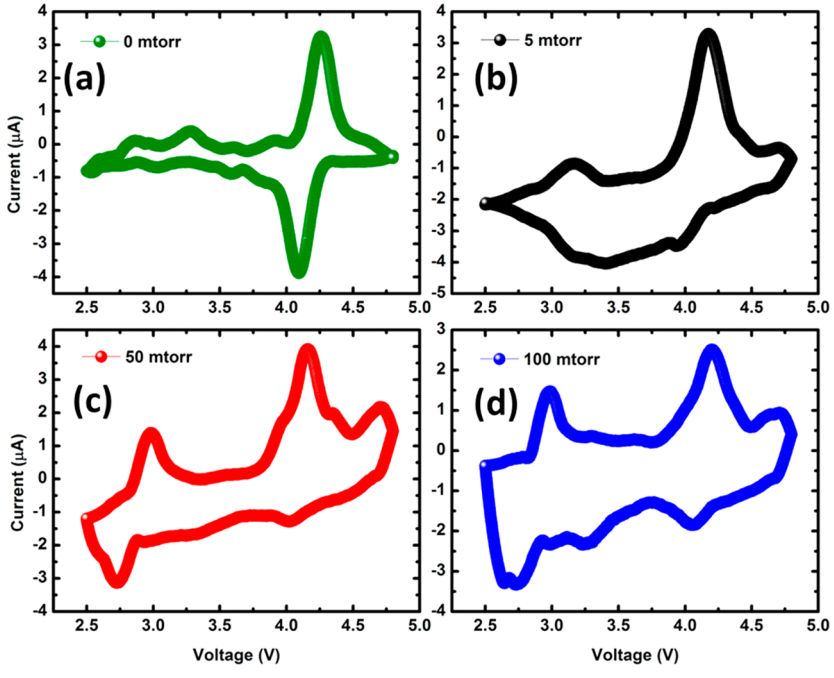

Figure 6. Cyclic voltammetry obtained for films deposited at (a) 0, (b) 5, (c) 50, and (d) 100 mTorr.

DOI: 10.1021/am5071305
ACS Appl. Mater. Interfaces 2015, 7, 2433–2438

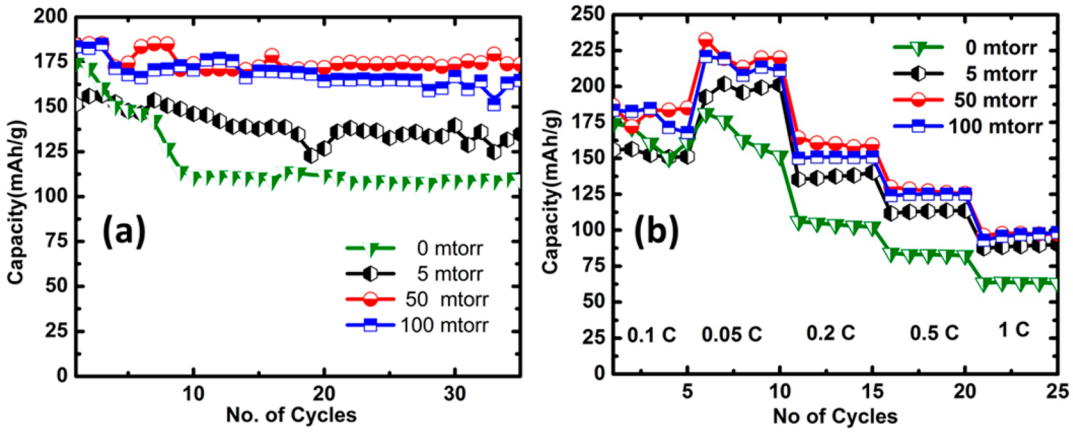

Figure 7. (a) Cycling capacity and (b) rate capability of films deposited under different conditions.

for improved ion dynamics addressing one of the key limitations of Li_2MnO_3 cathodes.[11]

This preliminary study has demonstrated that it is possible to design a wide range of stoichiometric derivatives of the native Li_2MnO_3 with the proposed thin film growth technique. We believe that the formation of MnO_2 is consistent with extreme Li and O deficiency and is a result of two different processes. It has been widely reported that a spinel-like phase formation occurs during the activation process driven by Li_2O extraction.[9,22] Lithium deficiency in the Li layer promotes Mn ions from the transition metal layer to occupy some of these sites. This leads to formation of a spinel-like electrochemically active phase. Further extraction of Li_2O as simulated by the vacuum sample in this work leads to formation of the spinel λ-MnO_2 phase. The layered Li_2MnO_3 that is not converted to the spinel-like activated phase during the deposition converts to α-MnO_2 due to Li and O loss. Both these mechanisms are consistent with experimental acid etching results reported by Shao-Horn and co-workers.[23] To the best of our knowledge, this is the first report on the formation of MnO_2 with in situ extraction of Li_2O. The MnO_2 formation was simulated in this process and shown to be a strong function of Li and O removal; however it is independent of variables such as, presence of H^+, diffusion rate, etc., introduced during other traditional Li_2O removal methods. α-MnO_2 suffers severe structural degradation upon lithiation during electrochemical cycling.[24] This likely contributed to the poor cycling performance of the 0 mTorr sample. In fact, the capacity obtained after cycling in this work agrees well with results reported in literature for α-MnO_2.[25] We had shown in our previous work that in Li-rich chemistries cathodes with nanodomains of Li_2MnO_3 perform better than those with much smaller and uniform distribution of Li_2MnO_3 in the $LiMO_2$ matrix.[15] It is conceivable that better Li mobility in the latter hastens the formation of MnO_2 resulting in the poor performance observed. The good performance of the 100 mTorr sample is partly due to the use of Li anode in the test cells, which compensates for Li deficiency during initial cycling. As shown in the 50 mTorr case, defects can form even in samples without oxygen deficiency. A possible way to achieve this effect in bulk synthesis process would be employing low temperature synthesis techniques. While traditionally electrochemical activity in Li_2MnO_3 has been linked to oxygen defects, in other Mn-based cathodes, oxygen deficiency has been linked with capacity decay.[26] In this context, electrochemical activity in samples with slight oxygen excess could be promising. In fact, one of the proposed techniques to stabilize α-MnO_2 cathodes is to use lithia-stabilized MnO_2.[25]Fine tuning Li_2O extraction to directly synthesize the "activated" Li_2MnO_3 phase formation should be theoretically possible. Such further investigation would be useful to study various aspects like preactivation, role of proton exchange, and detailed mechanism resulting in the irreversible capacity loss.

CONCLUSION

In summary, we successfully demonstrated the synthesis of Li_2MnO_3 with a wide range of stoichiometries by selectively removing Li and O in situ, with this unique approach. MnO_2 formation is shown to be a direct result of stoichiometry variation, independent of other mechanisms that occur during electrochemical cycling. A large reduction in Li and O content leads to formation of MnO_2 phase that gives a discharge capacity of 112 mAh g^{-1} after 30 cycles. The distinct electrochemical behavior and capacity reduction can be directly correlated to MnO_2 formation in Li_2MnO_3 cathodes. Cathodes with a slight excess of Li and O deposited at 50 mTorr of oxygen partial pressure showed localized defects and gave an excellent capacity of 225 mAh g^{-1} at 0.05 C. The results present a likely reason for poor performance of some Li-rich cathodes. This thin film cathode growth technique can be applied to adjust the Li and O contents of the film independently to investigate various important mechanisms, including Li_2MnO_3 preactivation, modifying film kinetics, and investigating phase transformation like monoclinic to spinel phases.

AUTHOR INFORMATION

Corresponding Author

*Haiyan Wang. E-mail: wangh@ece.tamu.edu.

Author Contributions

The manuscript was written through contributions of all authors. All authors have given approval to the final version of the manuscript.

Funding

The work is partially funded by the National Science Foundation, DMR-0846504 (for high resolution STEM analysis) and DMR-1401266 (for thin film growth effort). A portion of the electron microscopy experiments was performed at National Center for Electron Microscopy (NCEM), which is supported by the Office of Science, Office of Basic Energy Sciences of the US Department of Energy under Contract No. DE-AC02-05CH11231. The FE-SEM acquisition was sup-

DOI: 10.1021/am5071305
ACS Appl. Mater. Interfaces 2015, 7, 2433−2438

ported by NSF DBI-0116835, the VP of Research office, and Texas A & M Engineering Experiment Station.

Notes

The authors declare no competing financial interest.

REFERENCES

(1) Goodenough, J. B.; Park, K.-S. The Li-Ion Rechargeable Battery: A Perspective. *J. Am. Chem. Soc.* **2013**, *135*, 1167−1176.

(2) Bruce, P. G.; Armstrong, A. R.; Gitzendanner, R. L. New Intercalation Compounds for Lithium Batteries: Layered $LiMnO_2$. *J. Mater. Chem.* **1999**, *9*, 193−198.

(3) Shaju, K. M.; Bruce, P. G. A Stoichiometric Nano-$LiMn_2O_4$ Spinel Electrode Exhibiting High Power and Stable Cycling. *Chem. Mater.* **2008**, *20*, 5557−5562.

(4) Lanz, P.; Villevieille, C.; Novák, P. Electrochemical Activation of Li_2MnO_3 at Elevated Temperature Investigated by In-Situ Raman Microscopy. *Electrochim. Acta* **2013**, *109*, 426−432.

(5) Yabuuchi, N.; Yoshii, K.; Myung, S.-T.; Nakai, I.; Komaba, S. Detailed Studies of a High-Capacity Electrode Material for Rechargeable Batteries, Li_2MnO_3−$LiCo_{1/3}Ni_{1/3}Mn_{1/3}O_2$. *J. Am. Chem. Soc.* **2011**, *133*, 4404−4419.

(6) Kalyani, P.; Chitra, S.; Mohan, T.; Gopukumar, S. Lithium Metal Rechargeable Cells using Li_2MnO_3 as the Positive Electrode. *J. Power Sources* **1999**, *80*, 103−106.

(7) Gao, Y.; Ma, J.; Wang, X.; Lu, X.; Bai, Y.; Wang, Z.; Chena, L. Improved Electron/Li-Ion Transport and Oxygen Stability of Mo-Doped Li_2MnO_3. *J. Mater. Chem. A* **2014**, *2*, 4811.

(8) Rana, J.; Stan, M.; Kloepsch, R.; Li, J.; Schumacher, G.; Welter, E.; Zizak, I.; Banhart, J.; Winter, M. Structural Changes in Li_2MnO_3 Cathode Material for Li-Ion Batteries. *Adv. Energy Mater.* **2014**, *4*, No. 1300998.

(9) Lee, E.; Persson, K. A. Structural and Chemical Evolution of the Layered Li-Excess Li_xMnO_3 as a Function of Li Content from First-Principles Calculations. *Adv. Energy Mater.* **2014**, *4*, No. 1400498, DOI: 10.1002/aenm.201400498.

(10) Ruprecht, B.; Wilkening, M.; Uecker, R.; Heitjans, P. Extremely Slow Li Ion Dynamics in Monoclinic Li_2TiO_3 Probing Macroscopic Jump Diffusion via 7Li NMR Stimulated Echoes. *Phys. Chem. Chem. Phys.* **2012**, *14*, 11974−11980.

(11) Fehr, Th.; Schmidbauer, E. Electrical Conductivity of Li_2TiO_3 Ceramics. *Solid State Ionics* **2007**, *178*, 35−41.

(12) Abouimrane, A.; Compton, O. C.; Deng, H.; Belharouak, I.; Dikin, D. A.; Nguyen, S. T.; Amine, K. Improved Rate Capability in a High-Capacity Layered Cathode Material via Thermal Reduction. *Electrochem. Solid-State Lett.* **2011**, *14*, A126−A129.

(13) Zhao, C.; Wang, X.; Liu, X.; Zhang, H.; Shen, Q. Mn−Ni Content-Dependent Structures and Electrochemical Behaviors of Serial $Li_{1.2}Ni_{0.13+x}Co_{0.13}Mn_{0.54-x}O_2$ as Lithium-Ion Battery Cathodes. *ACS Appl. Mater. Interfaces* **2014**, *6*, 2386−2392.

(14) Jacob, C.; Lynch, T.; Chen, A.; Jian, J.; Wang, H. Highly Textured $Li(Ni_{0.5}Mn_{0.3}Co_{0.2})O_2$ Thin Films on Stainless Steel as Cathode for Lithium-Ion Battery. *J. Power Sources* **2013**, *241*, 410−414.

(15) Jacob, C.; Jian, J.; Zhu, Y.; Su, Q.; Wang, H. A New Approach to Investigate Li_2MnO_3 and $Li(Ni_{0.5}Mn_{0.3}Co_{0.2})O_2$ Mixed Phase Cathode Materials. *J. Mater. Chem. A* **2014**, *2*, 2283−2289.

(16) Boulineau, A.; Croguennec, L.; Delmas, C.; Weill, F. Reinvestigation of Li_2MnO_3 Structure: Electron Diffraction and High Resolution TEM. *Chem. Mater.* **2009**, *21*, 4216−4222.

(17) Hy, S.; Felix, F.; Rick, J.; Su, W.-N.; Hwang, B. J. Direct In-Situ Observation of Li_2O Evolution on Li-Rich High Capacity Cathode Material, $Li[Ni_{(x)}Li_{((1-2x)/3)}Mn_{((2-x)/3)}]O_2$ $(0 \le x \le 0.5)$. *J. Am. Chem. Soc.* **2014**, *136*, 999−1007.

(18) Ohzuku, T.; Nagayama, M.; Tsujia, K.; Ariyoshi, K. High-Capacity Lithium Insertion Materials of Lithium Nickel Manganese Oxides for Advanced Lithium-Ion Batteries: Toward Rechargeable Capacity more than 300 mA h g^{-1}. *J. Mater. Chem.* **2011**, *21*, 10179−10188.

(19) Rossouw, M. H.; Thackeray, M. M. Lithium Manganese Oxides from Li_2MnO_3 for Rechargeable Lithium Ion Battery Applications. *Mater. Res. Bull.* **1991**, *26*, 463−473.

(20) Wu, X.; Li, H.; Fei, H.; Zheng, C.; Wei, M. Facile Synthesis of Li_2MnO_3 Nanowires for Lithium-Ion Battery Cathodes. *New J. Chem.* **2014**, *38*, 584−587.

(21) Amalraj, S. F.; Markovsky, B.; Sharon, D.; Talianker, M.; Zinigrad, E.; Persky, R.; Haik, O.; Grinblat, J.; Lampert, J.; Dobrick, M. S.; Garsuch, A.; Burlaka, L.; Aurbach, D. Study of the Electrochemical Behavior of the "Inactive" Li_2MnO_3. *Electrochim. Acta* **2012**, *78*, 32−39.

(22) Yu, D. Y. W.; Yanagida, K.; Kato, Y.; Nakamura, H. Electrochemical Activities in Li_2MnO_3. *J. Electrochem. Soc.* **2009**, *156*, A417−A424.

(23) Horn, Y. S.; Ein, E. Y.; Robertson, A. D.; Averi, I. W. F.; Hackney, S. A.; Howard, W. F., Jr. Morphology Modification and Delithiation Mechanisms of $LiMn_2O_4$ and Li_2MnO_3 by Acid Digestion. *J. Electrochem. Soc.* **1998**, *145*, 16−23.

(24) Tompsett, D. A.; Islam, M. S. Electrochemistry of Hollandite α-MnO_2: Li-ion and Na-ion Insertion and Li_2O Incorporation. *Chem. Mater.* **2013**, *25*, 2515−2526.

(25) Johnson, C. S.; Mansueto, M. F.; Thackeray, M. M.; Horn, Y.S.-; Hackney, J. S. A. Stabilized Alpha-MnO_2 Electrodes for Rechargeable 3 V Lithium Batteries. *J. Electrochem. Soc.* **1997**, *144*, 2279−2283.

(26) Xia, Y.; Sakai, T.; Fujieda, T.; Yang, X. Q.; Sun, X.; Ma, Z. F.; McBreen, J.; Yoshio, M. Correlating Capacity Fading and Structural Changes in $Li_{1+y}Mn_{2-y}O_{4-\delta}$ Spinel Cathode Materials: A Systematic Study on the Effects of Li/Mn Ratio and Oxygen Deficiency. *J. Electrochem. Soc.* **2001**, *148*, A723−A729.

DOI: 10.1021/am5071305
ACS Appl. Mater. Interfaces 2015, 7, 2433−2438